Table IV. Experimental and Scaled[a] Theoretical Vibrational Fundamental Frequencies (in cm^{-1})

molecule		ν_1	ν_2	ν_3
$SiCl_2$	expt[6]	512.5	202.2	501.4
	calcd	505.5	204.1	501.0
$SiBr_2$	expt[6]	402.6	*b*	399.5
	calcd	395.9	128.2	394.6
$GeCl_2$	expt[4]	396	*b*	372
	calcd	400.8	168.7	384.2
$GeBr_2$	expt[9]	286	110	276
	calcd	284.8	109.4	278.1

[a] Scale factors: 0.870 for stretches and 0.918 for bends. [b] Not observed experimentally.

Table V. Scaled Theoretical Fundamental Vibrational Frequencies and Intensities of *cis*-Ge_2Br_4 (in cm^{-1} and km mol^{-1}, Respectively)

	symmetry	description	freq	intens
ν_1	a_1	terminal str	318.0	104.0
ν_2	b_1	terminal str	309.0	8.5
ν_3	a_1	ring str/terminal bend	201.5	0.6
ν_4	b_2	ring str	194.8	52.4
ν_5	b_1	ring str	187.1	171.8
ν_6	a_1	ring def/ring str	144.4	0.9
ν_7	b_1	terminal bend	96.4	1.0
ν_8	a_1	ring def/terminal bend	94.6	0.2
ν_9	b_2	terminal bend	92.8	0.3
ν_{10}	a_2	terminal bend	84.7	0.0
ν_{11}	a_2	ring str	64.9	0.0
ν_{12}	a_1	ring puckering	15.4	0.1

agreement with the known experimental frequencies. The correct assignment of the two close-lying stretching frequencies in these compounds has not been quite resolved.[5,8] Unfortunately, chlorine isotopic data are of little help.[5,8] Our calculations predict that the totally symmetrical vibration, ν_1 is higher than ν_3 in each case. This agrees with the latest assignment of Miller and Andrews[4] and their earlier preference based on analogy with $SnCl_2$.[8]

We also determined the fundamental vibrational frequencies and intensities of the bridged cis dimer Ge_2Br_4 to assist in the assignment of any future infrared data. These calculations were done by using the program package CADPAC.[23] The results of this study are shown in Table V. We predict three strong infrared bands, at 318, 195 and 187 cm^{-1}, and a number of weaker ones. The observation of the three strong bands near their predicted positions would constitute, in our opinion, conclusive proof for the bridged structure of the dimer, Ge_2Br_4. No calculations have been performed for the trans form, but in view of the small splitting of the terminal Ge-Br frequencies (9 cm^{-1}), the position of the three strong infrared bands should be nearly the same.

Conclusions

Our study shows that the triplet state is not energetically accessible at 600 °C and therefore is not a possible model for the electron diffraction data obtained. The most likely model is the presence of a halogen-bridged dimer species of $GeBr_2$. The dimers, Ge_2Br_4 and Ge_2Cl_4, are probably bound by a dimerization energy of less than 40 kJ/mol. Continuing study of the matrix-infrared spectrum of the system in question should be completed in order to positively identify all species present. Our prediction of the experimental spectrum of Ge_2Br_4 should assist in this identification.

Acknowledgment. This project was supported in part by the National Science Foundation (Grant CHE-8500387). We are thankful to the J. W. Fulbright College of Arts and Sciences for the Fulbright College-Clare Hall Cambridge Dissertation Fellowship, which was awarded to J.M.C. for 1 year of research in Cambridge, England, where part of this study was completed. J.M.C. wishes to thank Dr. N. C. Handy and R. D. Amos for their help and advice and the use of their computing facilities. J.M.C. also wishes to extend a special thanks to Clare Hall, Cambridge, England, for their hospitality.

(23) Amos, R. D.; Rice, J. E. "CADPAC: The Cambridge Analytic Derivatives Package", issue 4.0; University of Cambridge, 1987.

Contribution from the Anorganisch-Chemisches Institut, Universität Münster, D-4400 Münster, West Germany

Band Structure and Bonding of $Er_8Rh_5C_{12}$ and Other Carbides with C_2 Pairs

Stephen Lee,* Wolfgang Jeitschko, and Rolf-Dieter Hoffmann

Received September 15, 1988

The electronic structure of $Er_8Rh_5C_{12}$ is treated by using standard one-electron (extended Hückel) calculations that rationalize the varying Rh-C distances within the $[Rh_5C_{12}]^{24-}$ polyanion as well as the various Rh-C-Rh and Rh-C-C bond angles. Two separate models are contrasted. In the first the erbium atoms are treated as mere three-electron donors, while in the second the erbium orbitals are included. While some geometric features of $Er_8Rh_5C_{12}$ may be understood purely with the first model, others can be rationalized only with the active participation of the erbium atomic orbitals. For comparison the electronic structures of several hypothetical and real RhC_2^{3-} systems are studied including the polyanion of the $CeNiC_2$ type structure.

Introduction

In recent years a great number of ternary rare-earth transition-metal carbides have been synthesized.[1] The compound $Er_8Rh_5C_{12}$, whose synthesis and structure was reported in a previous paper,[2] is a typical example of such a compound. Little work has yet been done to characterize the band structure of these carbides. Here we report on the electronic structure of $Er_8Rh_5C_{12}$ by using a standard one-electron treatment. The especial advantage of the $Er_8Rh_5C_{12}$ system is that while the system is small enough to be amenable to one electron (extended Hückel) calculations,[3] it is also large enough to afford a diverse set of bond distances and bond angles. These geometrical variables are used throughout this work to assess the accuracy and utility of our simple electronic model.

Table I. Bond Lengths (pm) and Bond Angles (deg) in the Rh_5C_{12} Unit of $Er_8Rh_5C_{12}$[a]

Rh1-Cl (d_1)	193.7 (11)	Rh1-Cl1-C2 (θ_1)	167.9 (9)
Rh2-C2 (d_2)	203.8 (11)	Rh2-C2-C1 (θ_2)	149.2 (9)
Rh2-C3 (d_3)	200.8 (10)	Rh3-C3C4 (θ_3)	135.7 (7)
Rh3-C3 (d_4)	209.6 (10)	Rh3-C5-C6 (θ_4)	126.1 (8)
Rh3-C5 (d_5)	230.4 (12)	C1-Rh1-C1 (ϕ_1)	180.0 (0)
C1-C2 (l_1)	126.9 (16)	C2-Rh2-C3 (ϕ_2)	171.1 (4)
C3-C4 (l_2)	132.2 (14)	C3-Rh3-C5 (ϕ_3)	104.2 (4)
C5-C6 (l_3)	133.0 (16)		
Rh2-Rh3	270.8 (1)		

[a] Standard deviations in the position of the least significant digit are given in parentheses; d_i, l_i, θ_i, and ϕ_i all refer to the bonds and angles as shown in Figure 1.

* To whom correspondence should be addressed at the Department of Chemistry, University of Michigan, Ann Arbor, MI 48109.

0020-1669/89/1328-4094$01.50/0

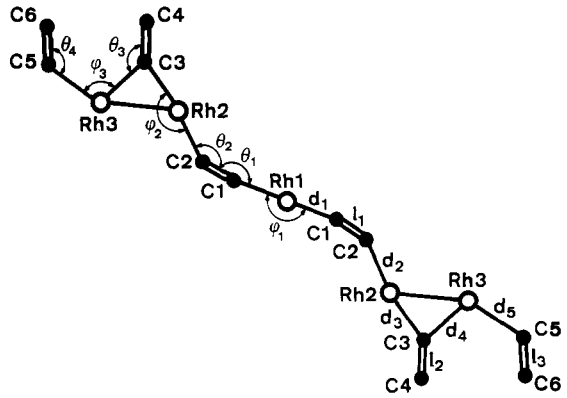

Figure 1. The Rh_5C_{12} unit of $Er_8Rh_5C_{12}$. It is planar and has an inversion center at Rh1. The values of the bond distances d_i, l_i and the angles θ_i, ϕ_i are listed in Table I.

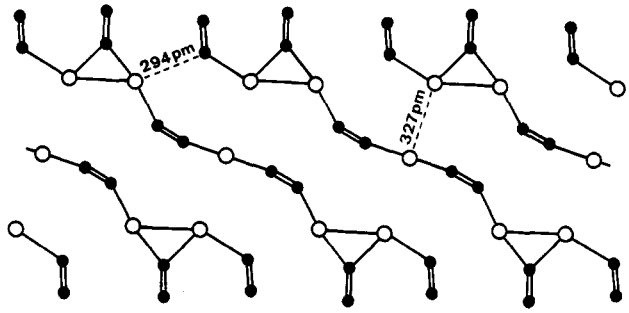

Figure 2. Rh_5C_{12} clusters forming a wide one-dimensional ribbon. The shortest interatomic distances between adjacent Rh_5C_{12} "polyanions" occur within these ribbons. They are indicated by broken lines. The Rh_5C_{12} units are interconnected in all three dimensions by Er atoms as shown in Figure 8.

The $Er_8Rh_5C_{12}$ structure is composed of elongated planar Rh_5C_{12} moieties (Figure 1, Table I). The shortest distances between adjacent Rh_5C_{12} clusters are a Rh–C distance of 294 pm and a Rh–Rh distance of 327 pm. Hence, the Rh_5C_{12} units may be treated as isolated from each other (Figure 2). Within each Rh_5C_{12} unit the Rh atoms are two-coordinated to carbon, and the carbon atoms (as in several other ternary rare-earth transition-metal carbides) form C_2 pairs. Finally, there are two Rh–Rh bonds of 270.8 pm/Rh_5C_{12} unit.

Among the great number of geometrical features of the Rh_5C_{12} cluster, the following are the particular concern of this article:

1. In contrast to most other rare-earth transition-metal ethylenic carbides, the coordination number of the transition metal for bonding to the carbon atoms is low. As is shown in Table II, $Er_8Rh_5C_{12}$ is that member of this family of compounds with the lowest coordination numbers of the transition metal and carbon atoms for bonding to each other.

2. The Rh–C bond distances vary from 194 pm to 230 pm. The longest Rh–C distances are found at the ends of the Rh_5C_{12} chain. The bond lengths become progressively shorter as one approaches the center of the moiety. There is a similar trend in C–C bond distances (Table I).

3. The Rh–C–C and C–Rh–C angles are near 180° at the center of the Rh_5C_{12} chain. As one progresses to the edges of the chain, both Rh–C–C and C–Rh–C angles become increasingly acute.

Table II. Coordination Numbers in Rare-Earth and Actinoid Transition-Metal (T) Carbides with C_2 Pairs

structure type (further examples) with ref no.	carbon neighbors of T atom	T neighbors of carbon atoms	electron count[b]
$CeNiC_2$[1a] ($DyFeC_2$,[1b] $DyCoC_2$,[1b] $DyNiC_2$,[1b] $SmRhC_2$[1c])	4	2	9–11
$CeCoC_2$[1d]	4	2	10
$ScCoC_2$[1e] ($ScFeC_2$,[1e] $ScNiC_2$,[1e] $UFeC_2$,[1f] $UCoC_2$,[1f] $UNiC_2$[1f])	4	0, 4	9–11
$CeRhC_2$[1c] ($LaRhC_2$[1c])	4	2	10
$Er_{10}Ru_{10}C_{19}$[1g]	4	2, 3, 6[a]	8.8
Sc_3CoC_4[1h]	4	1	14
U_2NiC_3[1i]	4	0, 2[a]	10
Er_2FeC_4[1j]	4	0, 2	10
$La_{12}Re_5C_{15}$[1k]	3	0, 1, 2[a]	5.8
$La_2Ni_5C_3$[1l]	2	2, 4[a]	10
$Er_8Rh_5C_{12}$[2]	2	0, 1, 2	11.4

[a] These compounds in addition to the C_2 pairs also contain carbon atoms that do not form pairs. For such systems the MO analysis given in the text must be modified. We consider these modifications in a forthcoming paper.[6] [b] Number of electrons per T atom in T atom d and/or C_2 π^* orbitals.

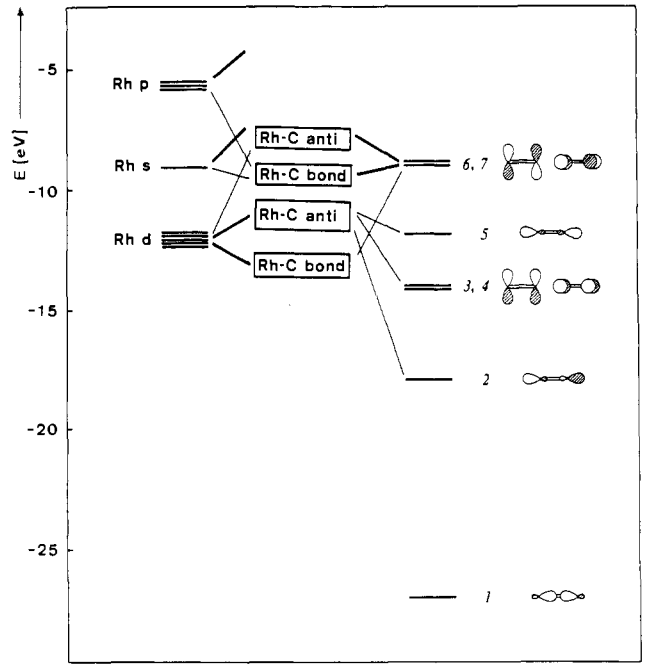

Figure 3. Interaction of the Rh and C_2 fragments in ethylene type rare-earth-metal rhodium carbides. On the left we place the Rh atomic orbitals, and on the right we place the C_2 fragment orbitals. **1**, **2**, and **5** are carbon s and p hybrids. As the overlap of the Rh s orbitals with **2**–**7** is stronger than the Rh d overlap, in general the s band is shifted above the C_2 π^* and Rh d bands. (Of course there is a great deal of s and p character mixed into the lower bands, as is discussed in the text.) The principal orbital provenance of each block is indicated by heavy lines. The qualitative picture here may be compared to the calculations shown in Figure 6.

Rh and C_2 Fragments

In accounting for these various geometrical trends, it will be found useful to use a fragment molecular orbital approach.[4] The

(1) (a) Bodak, O.-I.; Marusin, E. P. *Dokl. Akad. Nauk Ukr. S.S.R., Ser. A* **1979**, *12*, 1048. (b) Jeitschko, W.; Gerss, M. H. *J. Less-Common Met.* **1986**, *116*, 147. (c) Hoffmann, R.-D.; Jeitschko, W. *Z. Kristallogr.* **1988**, *182*, 137. (d) Bodak, O.-I.; Marusin, E. P.; Bruskov, V. A. *Sov. Phys. Crystallogr.* **1980**, *25*, 355. (e) Marusin, E. P.; Bodak, O.-I.; Tsokol, A. O.; Baivel'man, M. G. *Sov. Phys. Crystallogr.* **1985**, *30*, 340. (f) Gerss, M. H.; Jeitschko, W. *Mater. Res. Bull.* **1986**, *21*, 209. (g) Hoffmann, R.-D.; Jeitschko, W. *Z. Kristallogr.* **1987**, *178*, 110. (h) Tsokol, A. O.; Bodak, O.-I.; Marusin, E. P. *Sov. Phys. Crystallogr.* **1986**, *31*, 466. (i) Gerss, M. H.; Jeitschko, W. *Z. Kristallogr.* **1986**, *175*, 203. (j) Gerss, M. H.; Jeitschko, W.; Boonk, L.; Nientiedt, J.; Grobe, J.; Mörsen, E.; Leson, A. *J. Solid State Chem.* **1987**, *70*, 19. (k) Block, G.; Jeitschko, W. *Z. Kristallogr.* **1987**, *178*, 25. (l) Tsokol', A. O.; Bodak, O.-I.; Marusin, E. P. *Sov. Phys. Crystallogr.* **1986**, *31*, 39.
(2) Hoffmann, R.-D.; Jeitschko, W.; Reehuis, M.; Lee, S. *Inorg. Chem.* **1989**, *28*, 934.
(3) Theoretical studies on solid-state carbides include: (a) Wijeyesekera, S. D.; Hoffmann, R. *Organometallics* **1984**, *3*, 949. (b) Hoffmann, R.; Li, J.; Wheeler, R. A. *J. Am. Chem. Soc.* **1987**, *109*, 6600. Also of interest are theoretical studies on rare-earth-metal–carbon–halogen phases. (c) Bullett, D. W. *Inorg. Chem.* **1985**, *24*, 3319. (d) Satpathy, S.; Anderson, O. K. *Inorg. Chem.* **1985**, *24*, 2604. (e) Miller, G. J.; Burdett, J. K.; Schwarz, C.; Simon, A. *Inorg. Chem.* **1986**, *25*, 4437. (f) Dudis, D. S.; Corbett, J. D. *Inorg. Chem.* **1987**, *26*, 1933.

strongest interactions in the system are between the two carbon atoms of each C_2 unit. Useful fragments therefore will be the carbon pairs in one fragment and the remaining Rh atoms in the other. The C_2 fragments each contain five bonding and nonbonding orbitals **1**–**5** (see also Figure 3), all of energy lower or

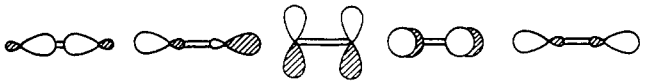

1 **2** **3** **4** **5**

equal to that of the Rh d orbitals (see the Appendix for atomic parameters). Approximately 3 eV above the Rh d orbitals lie the C_2 π^* orbitals **6** and **7**. These therefore have an energy similar

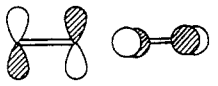

6 **7**

to that of the Rh s orbital. Finally the Rh p orbitals lie about 3 eV higher than the Rh s and C_2 π^* orbitals (The C_2 σ_{2p}^* orbitals are still higher in energy and are less important.) We show the relative position of the fragment orbitals in Figure 3. Of particular interest to us are the positions of the d block and the C_2 π^* block after the fragments have interacted. The bottom of the interacted d block will contain orbitals that are bonding to the C_2 π^* orbitals, while the top of the d block contains orbitals antibonding to the C_2 orbitals **2**–**5**. Similarly, the C_2 π^* band may be divided into low-lying orbitals that interact with Rh s and p orbitals and hence are Rh–C bonding and those that mix well with Rh d orbitals and hence are of higher energy and antibonding.

In many of the carbide phases shown in Table II, the number of transition metals and C_2 units is approximately equal. At this ratio of metal to carbon it is apparently unavoidable that the d block will be divided into bonding and antibonding parts as described above. There are only two C_2 π^* orbitals for every five d orbitals, and hence not all d orbitals can have Rh–C bonding character. Depending on the geometry of the system, it is at best possible for Rh s- and p-orbital mixing to remove much of the d-block antibonding character. Only for systems with a greater C_2 to metal ratio, as in Er_2FeC_4, should it be possible to generate a completely bonding metal d block.[5]

In contrast for the C_2 π^* block, with only two-fifths as many orbitals as the d block, it is possible to have purely antibonding Rh–C character. Only when the geometry of the structure does not allow consistently good d–π^* interaction will the bottom of the π^* block be of Rh–C bonding character. This is important. In many rare-earth transition-metal ethylenic carbides the Fermi level is at the top of the d block. Therefore, structural alternatives that waste Rh–C bonding potential in the unfilled C_2 π^* band will be energetically unfavorable in comparison to those that do not. Only for compounds (such as $Er_8Rh_5C_{12}$) that have higher electron counts are these criteria no longer valid. It is therefore worthwhile to establish what geometrical features are responsible for converting the C_2 π^* block into a purely Rh–C antibonding block.

Rh and C_2 Coordination Number

We find that the single most important geometrical feature, which controls the bonding or antibonding character of the π^* band, is the number of linkages between the Rh and C_2 units.[6] When the coordination number is high, we have a purely antibonding C_2 π^* band. In contrast for systems such as $Er_8Rh_5C_{12}$ where the coordination number is low, we have Rh–C bonding orbitals in the C_2 π^* block. This is so as the Rh s and p orbitals spatially overlap well with carbon orbitals. Indeed their overlaps are often twice as great as any d overlap integrals. Hence Rh s and p hybridization can overcome the initial Rh d–C_2 π^* antibond. Such hybridization though results in the formation of Rh orbital lobes that are outward pointing with respect to the C_2 units. When the coordination number is high, there is in general no direction into which the Rh orbital may bulge in such a manner. Let us consider a simple example of this effect. **8** is the layer

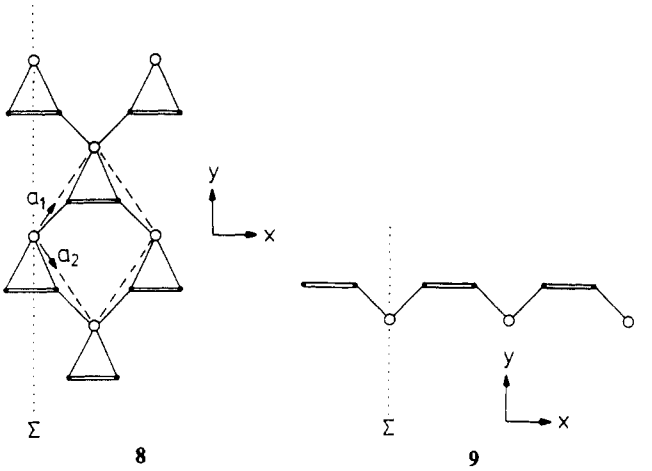

8 **9**

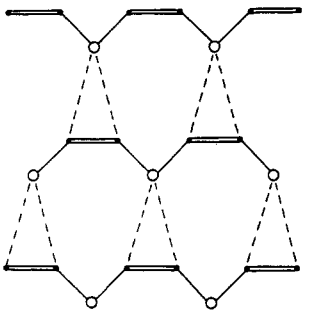

10

structure found in $SmRhC_2$[1c] ($CeNiC_2$ type structure), while **9** is a fragment of **8**. We illustrate in **10** how **8** and **9** are formed from one another.

In Figure 4 we contrast the band structures of these two systems. It may be seen that the C_2 π^* bands (these lie just above the 20 e/RhC_2 unit count) of **9** dip to much lower energies than those of **8**. Turning to the COOP curves[7] (Figure 5) of the Rh–C bond, we see that indeed the bottom of the C_2 π^* band is of Rh–C bonding character in **9** while of antibonding character in **8**.

Let us examine the orbital features responsible for this effect. For **9** at the points of special symmetry $\Gamma(0)$ and $Z(^1/_2)$ (we shall throughout this discussion limit ourselves to special symmetry points), our calculations show that the two low-lying π^* orbitals with net Rh–C bonding character are the molecular orbitals **11** and **12**. Their energies are denoted in Figure 4.

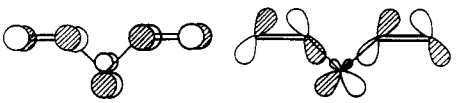

11 **12**

Their respective summed overlap populations are 0.152 and 0.244. When one compares these values with the total Rh–C

(4) See discussion in Chapter 13: Burdett, J. K. *Molecular Shapes*; J. Wiley: New York, 1980.

(5) Greater C_2 to metal ratio though, in no way ensures one of a purely Rh–C-bonding d block. Increasing the number of C_2 pairs also increases the number of low-lying C_2 orbitals as well. There are four outward-pointing C_2 bonding and nonbonding orbitals (**2**–**5**). At a metal to carbon ratio of 1:1 these four orbitals will leave five of the nine rhodium orbitals at lower energies. At higher ratios this is no longer assured.

(6) While the coordination number is the most important factor, other factors such as bond angles are also significant. We comment on this in our work on U_2NiC_3. See: Lee, S.; Jeitschko, W. To be submitted for publication.

(7) COOP is the crystal orbital overlap population weighted density of states. The function allows one to study the bonding character of all energy levels of the same energy. Earlier applications of this technique can be found in ref 3a. (a) Kertesz, M.; Hoffmann, R. *J. Am. Chem. Soc.* **1984**, *106*, 3453. (b) Saillard, J.-Y.; Hoffmann, R. *J. Am. Chem. Soc.* **1984**, *106*, 2006. (c) Hughbanks, T.; Hoffmann, R. *J. Am. Chem. Soc.* **1983**, *105*, 3528.

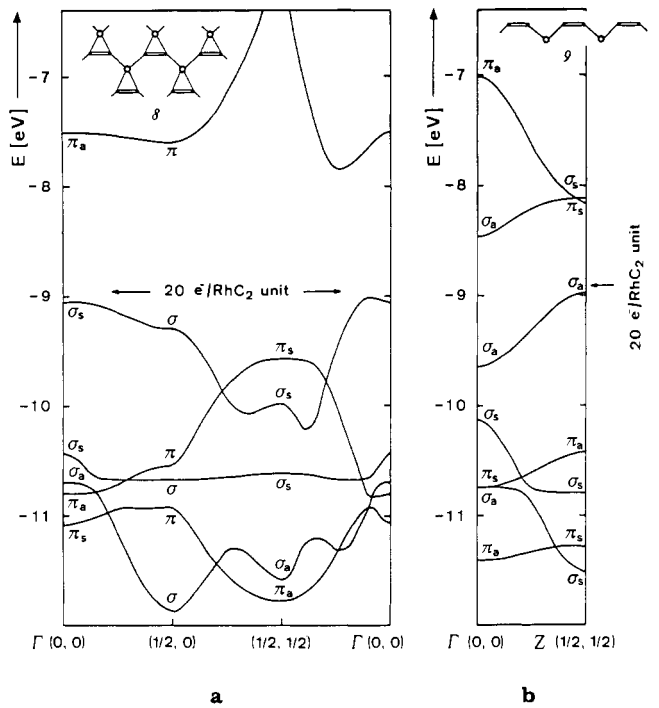

a b

Figure 4. Band structure of the polyanions **8** and **9**. In (a) the band structure of **8** is shown along lines running from left to right: (0,0) → $(x,0)$ → $(^1/_2,0)$ → $(^1/_2,x)$ → $(^1/_2,^1/_2)$ → $(^1/_2-x,^1/_2-x)$ → (0,0), where x increases in each region from 0 to $^1/_2$. The symmetry labels of the orbitals are shown for the special points. The σ and π labels refer to the traditional planar σ and π symmetry. At (0,0) and $(^1/_2,^1/_2)$ we have the added symmetry with respect to the mirror plane denoted by Σ in **8**. Orbitals symmetric with respect to Σ receive an s subindex, those antisymmetric an a index. The highest occupied orbital where there are 20 e/RhC_2 unit is denoted with an arrow. In (b) is shown the band structure of **9** from $\Gamma(0)$ to $Z(^1/_2)$. The same conventions apply here as in (a). In comparing the two structures note how the C_2 π^* bands in **9** dip to lower energies than in **8** (in **9** they start at −8.4 eV, while in **8** they start at −8 eV). As in **8** at both Γ and Z, we have the additional symmetry with respect to the Σ mirror plane.

summed overlap population for a d^{10} Fermi level of 0.578, one sees that these orbitals have significant Rh–C bonding potential. This bonding character is lost when chains of type **9** interact in the manner shown in **10**. To understand why this occurs, we consider how the orbitals **11** and **12**, which are respectively of $Z(\pi_s)$ and $\Gamma(\sigma_a)$ symmetry (see Figure 4), transform in going to the two-dimensional system **8**.

As before, we restrict our attention to k points of high symmetry. For the two-dimensional system **8** these are Γ, $(^1/_2,^1/_2)$, $(^1/_2,0)$, and $(0,^1/_2)$ (the latter two belong to the same star[8]), where we have used the crystal direct vectors shown in **8**. Corresponding to the one-dimensional $Z(\pi_s)$ and $\Gamma(\sigma_a)$ are $(^1/_2,0)\pi$, $\Gamma(\sigma_a)$, and $(^1/_2,^1/_2)\sigma_a$. First let us examine the $Z(\pi_s)$ to $(^1/_2,0)\pi$ transformation. In doing so let us at first not include any Rh s or p mixing. Under these constraints in contrast to **11** the $Z(\pi_s)$ C_2 π^* orbital is **13**. In going to $(^1/_2,0)\pi$ this orbital may now interact with

13

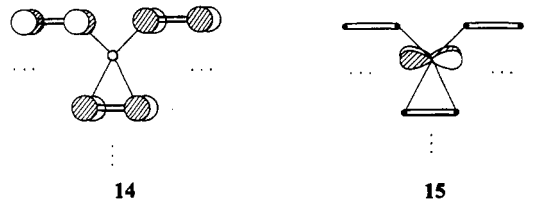

14 **15**

14 and **15**, as the Σ symmetry shown in **8** now transforms $(^1/_2,0)$ to $(0,^1/_2)$.[8] **14** is a C_2 π orbital, and **15**, a pure Rh d orbital. Recalling that the C_2 π^* fragment orbital lies higher in energy than the Rh d atomic orbital, we see that the C_2 π^* molecular orbital must be the most antibonding combination of the orbitals **13**–**15**. Thus, the $(^1/_2,0)\pi$ C_2 π^* orbital is of the form **16**. The

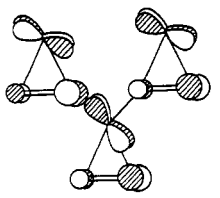

16

reason that the Rh–C bonding character of the $Z(\pi_s)$ C_2 π^* orbital **11** is lost is evident when one compares **13** to **16**. For **13** the inclusion of Rh π_π hybridization results in the hybrid orbital **11**, which has a net Rh–C bond. In **16** there is no free side into which the hybrid **11** may bulge and thus the chemical system is incapable of making a net Rh–C bond.

A similar analysis of $(0,0)\sigma_a$ and $(^1/_2,^1/_2)\sigma_a$ shows that the C_2 π^* functions (with no Rh s or p included) are of the form **17** and **18**. Again, there is no unoccupied space available for Rh s and

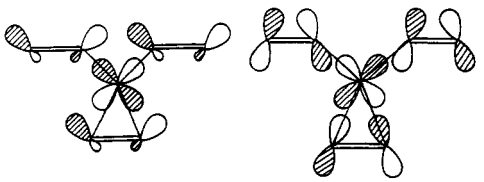

17 **18**

p hybridization, and again, there is no net Rh–C bonding character.

This effect, which we discussed in detail for this one specific case, is quite general.[9] In Figure 6 we show the COOP curves for a few other systems. It is only those systems with maximal planar coordination that have a purely Rh–C antibonding C_2 π^* block.

Finally, it should be noted that no formal proof of the importance of the Rh–C_2 coordination number to the form of the Rh–C COOP curve has been given. For example in our previous discussion we might have argued that it is the C_2 pair coordination that is responsible for the difference in the Rh–C COOP curves of **8** and **9**. While such an observation is important, and indeed may be used in understanding the newly discovered Sc_3CoC_4 structure, it cannot account for the difference in bonding character for the system shown in Figure 6b vs the one shown in Figure 6a. It is for this reason, after examining many systems both hypothetical and real (examples of this work are in Figure 6), that we have concluded the Rh–C_2 coordination number is the single most important factor in predicting the nature of the Rh–C COOP curves.

Effect of Erbium on the Coordination Number of Rh and the C_2 Fragment

As yet we have not included the rare-earth-metal atoms in our discussion. In systems with the Fermi level in the C_2 π^* block, these will play a considerable role. In such systems the rare-earth-metal s and d orbitals lie close to the Fermi level. For those systems in which there is Rh–C bonding character in the lower part of the C_2 π^* block, the bonding character can easily be spread across the whole band by rare-earth-metal interactions.[10]

(8) Bouckaert, L. P.; Smoluchowski, R.; Wigner, E. P. *Phys. Rev.* **1936**, *50*, 58.

(9) The relation between the number of bonding and nonbonding orbitals and the coordination number CN is well established. Well-known examples are the structures of the main group elements: e.g. Si (CN 4), P (CN 3), S (CN 2), Cl (CN 1), and the series Fe^{2+} (CN 6), Pd^{2+} (CN 4), and Hg^{2+} (CN 2). See: (a) Chapter 14 of ref 4 for a review of the applications of these ideas to cluster compounds. This relationship is applied to solid-state compounds in: (b) Burdett, J. K.; McLarnan, T. J. *Inorg. Chem.* **1982**, *21*, 1119.

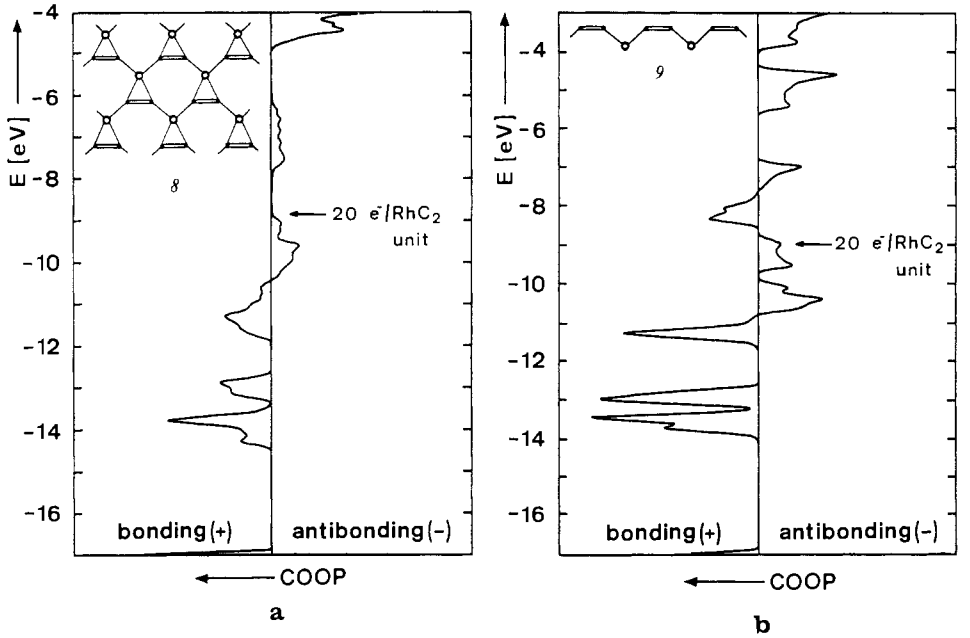

Figure 5. Rh–C COOP: population overlap of the Rh–C bond by energy level for two differently bonded RhC_2 polymers. Whenever the curve is positive, we have a net Rh–C bond at this energy level. Whenever it is negative, it is antibonding. Both curves are drawn for the 20 e/RhC_2 unit. Note that the **9** Rh–C COOP curve still has positive regions above the 20 e/RhC_2 unit level. We point out that the Rh–C antibonding regions that form the top of the d band are of bonding character with respect to the Er–Rh, Er–C, and C–C interactions.

Thus, Rh–C bonding and antibonding bands may overlap. By contrast, for those systems with the Fermi level at the top of the d block the situation is simpler. Rare-earth-metal interactions will not be able to reincorporate the Rh–C bonding character of the C_2 π^* block into the d block.[10] Hence, for systems with a filled d band and unfilled higher bands, high coordination is to be preferred.

This is borne out by Table II and Figure 6, where we see that all d^{10} electron count systems contain sufficiently high coordination so as to generate a purely Rh–C antibonding C_2 π^* block. Systems with higher Fermi levels do not have to maintain the high transition-metal coordination number (although they may maintain it, as the Sc_3CoC_4 structure illustrates).

Bond Angles in $Er_8Rh_5C_{12}$

In the first section of this paper we noted that there is a wide range of Rh–C–C (θ_i) and C–Rh–C (ϕ_i) angles in the $Er_8Rh_5C_{12}$ system and that in general as one approaches the center of the Rh_5C_{12} unit, both the θ_i and ϕ_i angles become increasingly obtuse (see Table I). In Figure 7 we show how the total energy of the $[Rh_5C_{12}]^{24-}$ system is changed as we alter the various angles. In performing these calculations, we unfortunately are not able to include the Er atoms. As we shall see later, the Er atoms are highly coordinated to both the Rh and C atoms. Bond angle variations therefore result in changing Er–Rh and Er–C bond lengths. Unfortunately, in such cases the extended Hückel method does not give reliable results.[11] Despite the absence of the Er atoms, we find that the bond angles predicted by our calculations are in reasonable agreement with the observed angles. In the case of θ_1, θ_3, θ_4, ϕ_1, and ϕ_2 the deviation is 12, 7, 5, 0, and 18°, respectively. Only θ_2 and ϕ_3 are in error by 30–40°. The observed trends along the polyanionic chain in both Rh–C–C angles (θ_i's) and C–Rh–C angles (ϕ_i's) are also reproduced in the calculations. Thus, the predicted θ_i's range 130–180°, compared to the experimental range 126–168°, and the predicted ϕ_i's range 140–180° compared to the observed 104–180°. Thus, the extended Hückel method appears to be a viable method for understanding the bond angle variations.

Furthermore in many cases, the deviation between the experimental and calculated geometry can be rationalized as an effect of the Er atoms. In this simple rationalization we assume the Rh or C atoms to experience an additional force that pushes them away from the nearest of their Er neighbors. In Figure 8 we show the Er neighbors of the Rh_5C_{12} chain. We see for example that the C2 atom has two Er neighbors at 257 pm and another two at 289 pm. In this model the Er interaction therefore should shift the minimum energy configuration of θ_2 toward a more acute angle. A similar although smaller effect is seen for ϕ_2, where the six Er neighbors of Rh2 are by pairs at distances of 282, 307, and 309 pm. For θ_1 an even smaller effect is expected as C1 has four Er neighbors, two at 254 pm and two at 261 pm. Finally, for ϕ_1 there should be no net effect at all as Rh1 lies at an inversion center. These rationalizations correspond nicely to the observed deviations of 30, 18, 12, and 0° for respectively θ_2, ϕ_2, θ_1, and ϕ_1. The directions of the deviations are also correctly rationalized. One factor responsible for this good agreement is that for these four angles the pertinent Er atoms all lie alongside a more or less linear Rh1–C1–C2–Rh2 backbone. Thus, the Er atom positions couple in an obvious manner to the various bond angles. For the remaining angles we are not able to apply this simple model. In the remaining cases the Er–C and Er–Rh bonds are entangled not just with bond angles but with Rh–C and C–C bond distances as well. We are therefore not able to draw any conclusions about the serious deviation between experimental observation and theoretical prediction for ϕ_3. Nevertheless the overall correlations between observed and predicted θ and ϕ angles remain surprisingly good.

Molecular Orbital Basis of Angular Trends

In order to appreciate the molecular orbital basis for the angular preferences of Rh_5C_{12}, let us now first consider the model RhC_2 systems **19–22**. The study of these systems allows us to isolate the angular effects found in the center of the Rh_5C_{12} chain from those found at the cluster edges. In Figure 9 we contrast the stability of these four systems as a function of electron count. In Figure 10 we illustrate their corresponding band structures. As Figure 9 shows, at the electron counts of interest, 20–22 e/per RhC_2 unit, the linear configuration **19** is preferred. This is the same geometric preference we found in our studies on θ_1, θ_2, ϕ_1, and ϕ_2. It may furthermore be seen that the least energetically

(10) The rare-earth-metal C_2 π^* interaction may be so strong as to place the bonding rare-earth-metal C_2 π^* orbitals at energies near those we find for the transition-metal d block. Thus, in ref 3e the bonding C_2 π^* orbitals are found at −9 to −11 eV. In such a case our overall picture would have to include the rare-earth-metal interactions even when we have a 10 e/transition metal Fermi level.

(11) For a discussion of this problem, see: Burdett, J. K. *Struct. Bonding (Berlin)* **1987**, *65*, 29.

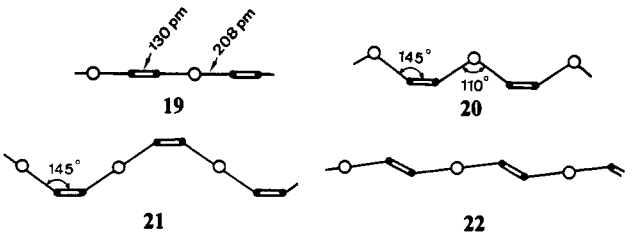

19 **20** **21** **22**

favorable system is **20**, where the C–Rh–C angle is not linear.

The molecular orbital basis for this effect is that in **19**, **21**, and **22** the Rh s orbital throughout k space is of the same symmetry as the most antibonding Rh d-block orbital. Thus, in these systems, the top of the d band is always readily stabilized by the s orbital. In the system **20** the most antibonding d orbital (ignoring Rh p mixing) at the special symmetry points Γ and Z are of the form **23** and **24**. These are of symmetry different from that of

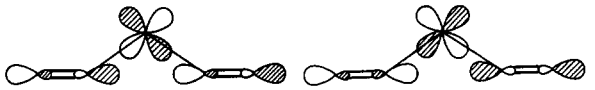

23 **24**

the Rh s orbital. Instead they are stabilized only by a Rh p orbital, which as it lies 3 to 4 eV higher than the s orbital, does not mix in as well. Indeed we see (Figure 10) that the top of the Rh d band in **20** lies almost 1 eV higher than in the other RhC_2 systems. It is this upward shift in the top of the d band that is principally responsible for the lack of stability of **20** with respect to the other systems at the 20 e/RhC_2 unit count.

By contrast the band structures of **19**, **21**, and **22** are much more closely related. There is no simple symmetry-based explanation that accounts for the difference in energy of these systems. One good way to understand the differences of energies in these systems is via the moment method.[12] We do not apply the method in a direct manner here. The orbital Coulombic values (H_{ii}) are spread over too wide an energy range for such a treatment. Instead we restrict our attention to those atomic orbitals that we know from our fragment approach to be of importance. Furthermore, we consider only σ orbitals, as it is these orbitals that are principally responsible for the various differences in electronic energy. We therefore consider only the restricted set comprised of the C orbitals **25**–**28** and the Rh d and s orbitals **29**–**31**. In **27** and **28**

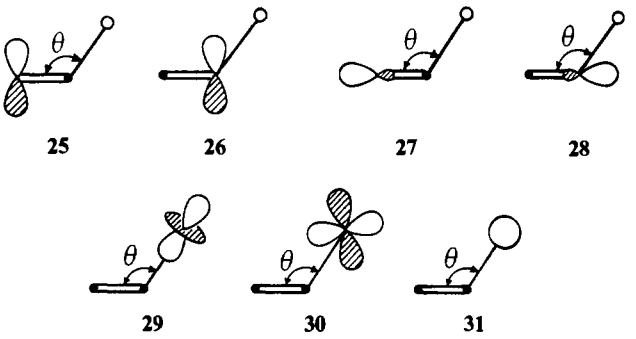

25 **26** **27** **28** **29** **30** **31**

the s and p hybrid $(2/\sqrt{5})(p + s/2)$ is chosen, which corresponds to the average hybridization found in the C_2 molecular orbitals shown earlier (**2** and **5**).

In Table III we give the respective H_{ii} values of these orbitals. We see that these orbitals lie reasonably close in energy. In Table IV we list the overlap integrals of these orbitals. We see that the ⟨**27**|**28**⟩ overlap integral is practically negligible. This is important, as therefore all fourth-moment contributions must arise from walks of length four involving **25** and **26**. It may be seen from Table IV that when $\theta = 145°$, the orbital **26** overlaps with the Rh orbitals much more strongly than when $\theta = 180°$. Indeed the μ_4 contribution[17] of θ angular dependent walks is 0.010 when $\theta = 145°$ and 0.001 when $\theta = 180°$. We therefore expect in the band center that a linear geometry is of lower energy. At 20 e/RhC_2 unit we have occupied five of the seven orbitals and therefore lie in this middle region. It may be seen that the results of Figure 9 confirm this prediction.

(12) (a) Cyrot-Lackmann, F. *J. Phys. C* **1972**, *5*, 300. (b) Burdett, J. K.; Lee, S. *J. Am. Chem. Soc.* **1985**, *107*, 3050.

Table III. Coulomb Integrals of Important Rh and C Orbitals

orbital	H_{ii}, eV	orbital	H_{ii}, eV
25, **26**	−11.0	**29**, **30**	−11.0
27, **28**	−13.4	**31**	−8.0

[a] Orbital numbers correspond to the pictures given in the text.

Table IV. Overlap Integrals of Important Rh and C Orbitals[a]

	|25⟩	|27⟩	|29⟩	|30⟩	|31⟩
			$\theta = 180°$ [b]		
⟨26|	0.286	0	0	0.124	0
⟨28|	0	−0.009	0.234	0	0.363
			$\theta = 145°$		
⟨26|	0.286	0	0.098	0.101	0.152
⟨28|	0	−0.009	0.206	0.063	0.321

[a] The overlap integrals are presented in matrix form; thus ⟨**26**|**25**⟩ = 0.286. [b] The angle θ refers to the angle portrayed between the C_2 pair and the Rh atom shown in **25**–**31**.

θ_4 Study

The preceding analyses account for the geometric preference of two-coordinate Rh and two-coordinate C_2 units that are bound to one another. The angles θ_1, θ_2, ϕ_1, and ϕ_2 may all be understood in these terms. We now turn to θ_4. Here again we have a C_2 unit (C5 and C6) that can rotate around its single Rh–C bond without breaking or making any Rh–C bonds. The Rh atom to which the C5–C6 pair is bound is of a sort different from those previously encountered. This Rh3 atom is bound to another Rh atom (Rh2) as well as to a C_2 pair. We therefore study the θ_4 variable from the viewpoint of the two C5–C6 fragments with the remaining Rh_5C_8 cluster. Figure 11 shows that the principal stabilizing interaction comes from orbitals near the Fermi energy of the Rh_5C_8 cluster with the C_2 π^* orbitals. It may be seen that it is the two most low-lying orbitals in the C_2 π^* band that are the most angular dependent.

The provenance of these two molecular orbitals are the σ_u and σ_g fragment orbitals of both the Rh_5C_8 unit as well as the two C5–C6 pairs. In **32** we show the Rh3 component of the σ_u and

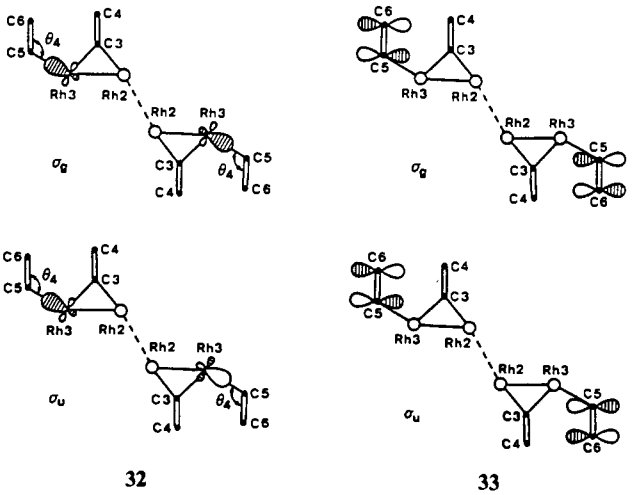

32 **33**

σ_g Rh_5C_8 fragment orbital, while in **33** we show the C_5–C_6 σ_u and σ_g fragment orbital. It can be seen that as the angle θ_4 approaches 90°, the interaction of these orbitals will improve. Hence, the linear geometry for θ_4 is not the lowest energy configuration.

Rh–C Bond Distances

Another geometric trend of the Rh_5C_{12} cluster is the tendency for the Rh–C bonds to lengthen as one approaches the edge of the chain (see Table I). This variation in bond lengths provides us with another test for our one-electron model. We compare in Table V the summed overlap populations to the actual Rh–C bond

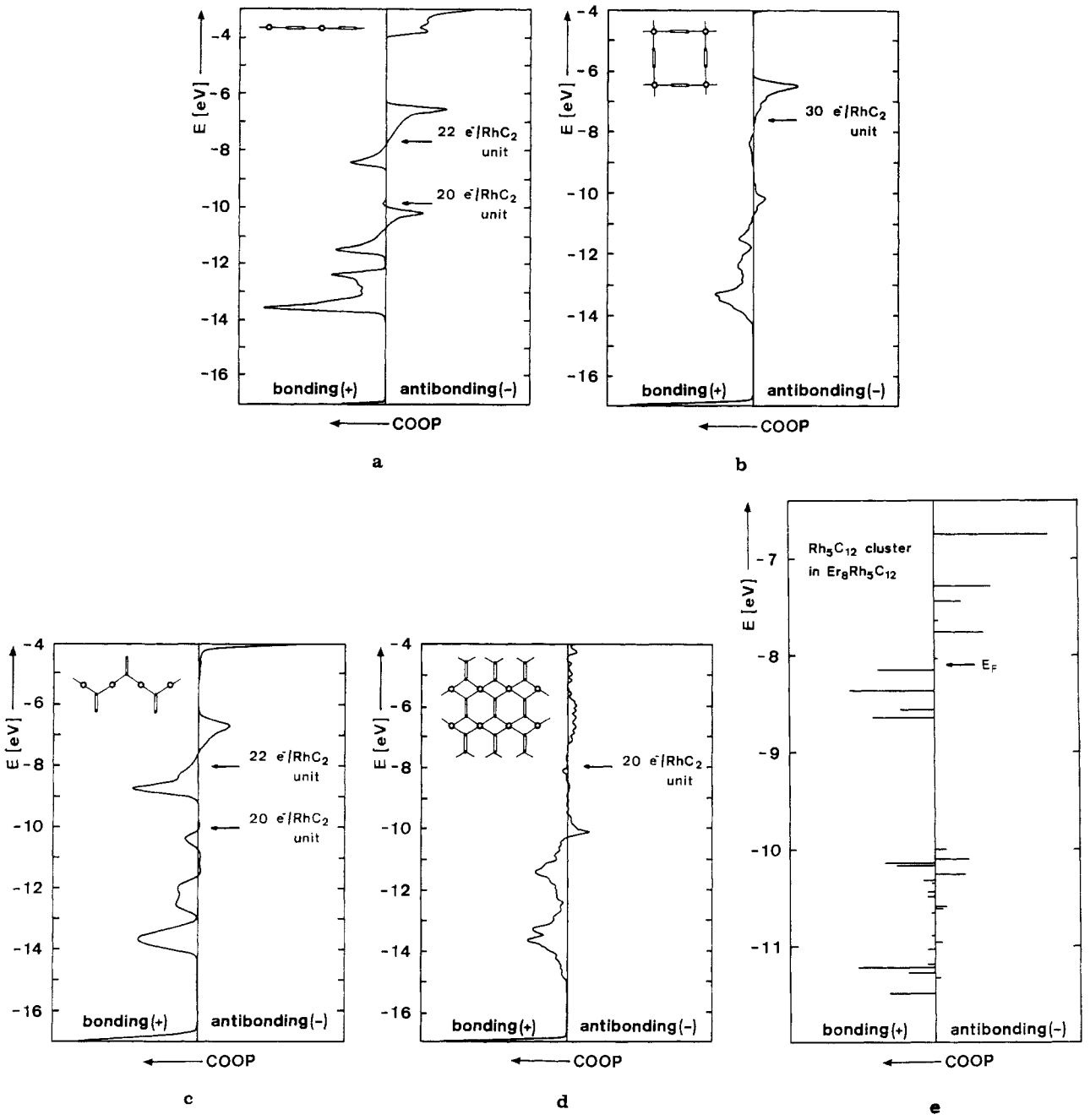

Figure 6. Rh–C COOP curves for various further Rh–C systems. The corresponding structures are always placed in the upper left-hand corner. Small open circles refer to Rh atoms, and small closed circles to the carbon atoms of the C_2 pairs. In (e) we show the Rh–C COOP curve for the actual $[Rh_5C_{12}]^{24-}$ cluster of $Er_8Rh_5C_{12}$. This last "curve" is for a molecule and hence has discrete narrow energy levels. The Fermi level for 117 valence electrons ((5 × 9) + (12 × 4) + 24) is indicated by an arrow.

distances. These results show that even when one idealizes the Rh–C and C–C bond distances, so that all Rh–C and C–C bonds are 208 and 130 pm, respectively, one already has a reasonable correlation between bond distances and bond overlap populations. The one exception is the Rh3–C5 (d_5) bond, whose bond overlap is close to that of the Rh2–C3 (d_3) bond but whose bond length is 30 pm longer. It is interesting that the d_5 bond corresponds to one leg of the ϕ_3 angle, whose anomalous behavior was discussed earlier. There we suggested that the angle anomalies between our calculated and experimental resuls could be correlated to the position of the Er atoms but were unable to explicitly include the Er atoms in our calculations. In studying Rh–C overlap populations, we are fortunately able to include the erbium atoms and hence are able to test this hypothesis. In Table V we show how the Rh–C overlap populations change as we include all nearest erbium neighbors of the Rh_5C_{12} cluster. Once the erbium atoms are included, the d_5 bond is found to have a much weaker bond overlap. Overall agreement between bond length and overlap is indeed excellent.

In order to understand some of the orbital features that are responsible for the improved agreement caused by the inclusion of the Er atoms, we consider the system **34**. It consists of a C_2

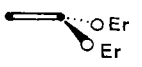

34

unit that has a pair of Er atoms lying near one but not the other carbon. Such geometrical units, as we shall see later, are quite frequent in the actual structure of $Er_8Rh_5C_{12}$. We study now how the Er atoms alter the C_2 fragment orbitals. For the sake of simplicity we ignore any C_2 σ–π mixing induced by the Er pair. In Figure 12a,b we draw convenient C_2 π atomic orbitals, which we will then interact with the Er atoms in order to generate the new fragment orbitals. We find that our resulting fragment C_2 orbitals are reasonably invariant to the type of orbitals placed on the Er atoms, and therefore for this simple example we consider only the Er s orbitals. (In the actual calculations the Er 6s, 6p, and the 5d orbitals were included.)

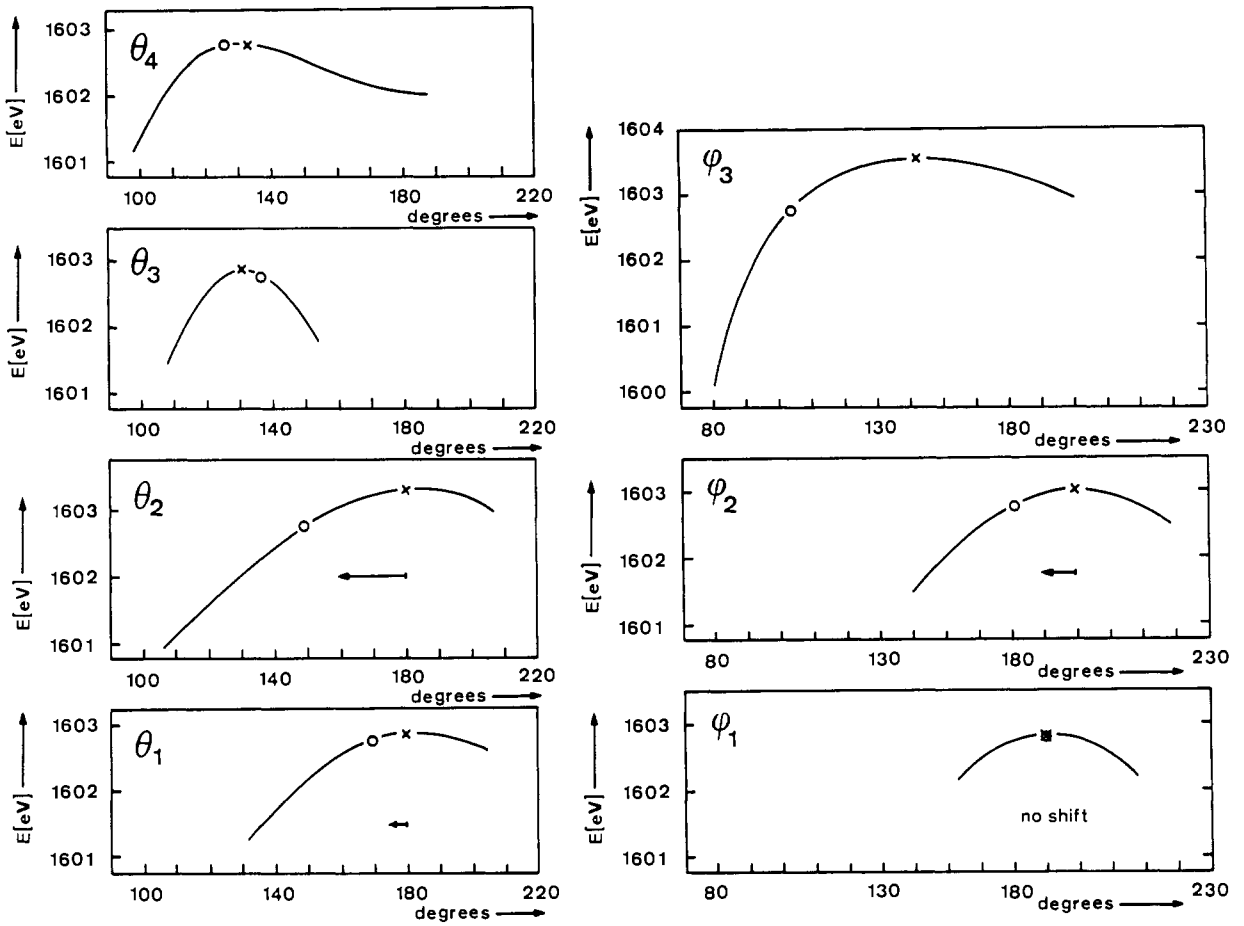

Figure 7. Binding energies as a function of the bond angles θ_i and ϕ_i. The total binding energy of the Rh_5C_{12} system is plotted as a function of the θ_i and ϕ_i angles. Only one angle is varied at a time. The greatest total binding energy is indicated with a cross; the observed value is denoted with a circle. For the four angles for which we have a steric model to account for the effect of the Er atoms, we indicate with an arrow the direction the minimum is expected to shift. The size of the arrow corresponds to the strength of the predicted steric effect of the Er atoms.

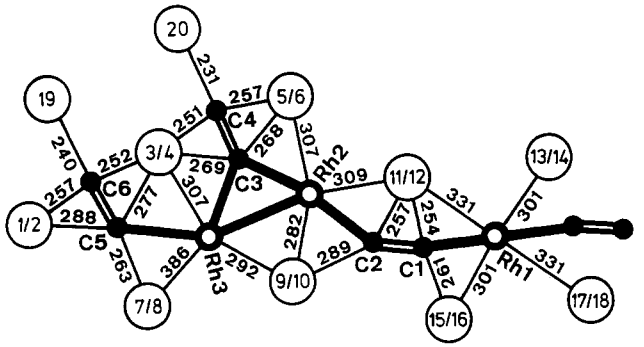

Figure 8. Erbium neighbors of the Rh_5C_{12} cluster. The cluster has an inversion center at the Rh1 atom, and the right-hand part of the cluster is not shown. The Er atoms are represented as large circles. Erbium atoms with one number are at the same height as the planar Rh_5C_{12} cluster. Where there are two numbers, two erbium atoms are superimposed; they are above and below the Rh_5C_{12} plane with the indicated bond distances (pm).

As Figure 12a,b shows, both π systems are analogous to the three-orbital π-allyl system.[13] Thus, had the Er s orbital the same H_{ii} value as the C p orbitals, the central molecular orbital would be of the form represented by **35** and **36**.

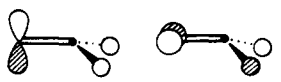

35 **36**

(13) See for instance: Fleming, I. *Frontier Orbitals and Organic Chemical Reactions*; J. Wiley: New York, 1976; p 19.

Table V. Summed Population Overlaps for the Rh–C Bonds in Rh_5C_{12}

Rh–C bond	exptl bond length, pm	bond overlaps[a]			
		A	B	C	D
d_1	194	0.741	0.896	0.620	0.678
d_2	204	0.668	0.665	0.566	0.531
d_3	201	0.616	0.672	0.620	0.595
d_4	210	0.502	0.476	0.444	0.458
d_5	230	0.608	0.470	0.300	0.325

[a] A: All Rh–C distances set equal to 208 pm. All C–C bond distances set at 130 pm. We do not report here the summed population overlaps for the C–C bonds. These overlaps change dramatically depending on the relative ordering of the several orbitals that lie near the Fermi level (see Figure 11). The average C–C summed overlap populations are roughly twice as big as the average Rh–C summed overlap population. The Rh2–Rh3 summed overlap population is smaller than the average Rh–C summed overlap population. B: Experimental Rh_5C_{12} geometry. No erbium atoms included. C: Fourteen Er atoms included (Er1–12,15,16). Due to the large size of the system we have eliminated the C4═C3Rh3—C5═C6 unit on the other side of the Rh_5C_{12} cluster. We assume that 7 e lie in the bands above the d block. We can estimate the error in this truncation by truncating the Rh_5C_{12} cluster and comparing it with the results of column A or B. The error is found to be on the average 3%. In the worse case the error is 8%. D: Same geometry as C. The Fermi level is taken to be at the top of the d block. The full "actual" prediction of the extended Hückel method therefore lies between the cases C and D.

Since erbium is much more electropositive, the true form of the central molecular orbital is **37** and **38**. These two fragment

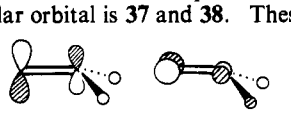

37 **38**

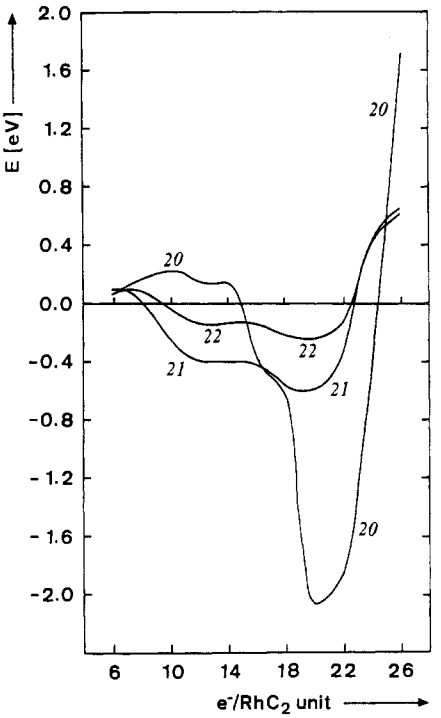

Figure 9. Relative energies of the RhC_2 chains **19–22**. The vertical coordinate shows the energy of the structures **20**, **21**, and **22** minus the energy of **19**. Thus, from 7 to 15 electrons per RhC_2 unit the structure **20** has the greatest binding energy. From 15 to 23 electrons—a range that includes all electron counts of interest—the linear structure **19** has the greatest electronic binding energy.

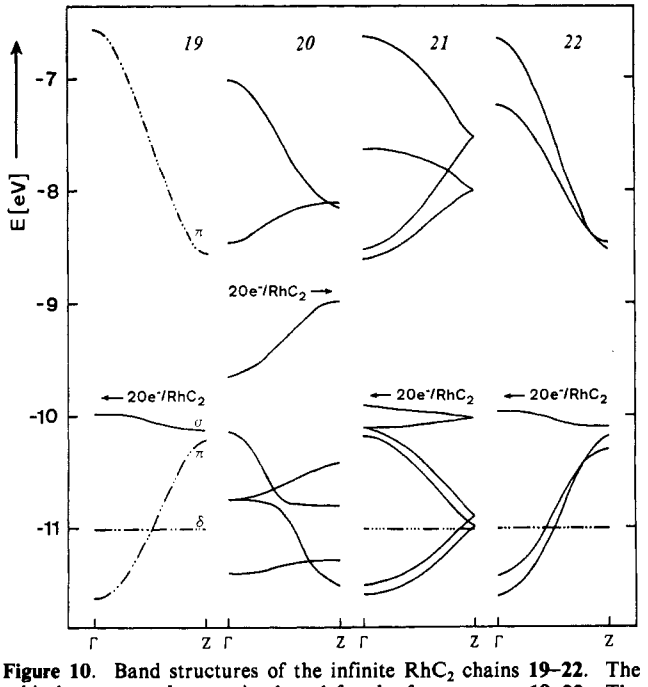

Figure 10. Band structures of the infinite RhC_2 chains **19–22**. The orbital energy vs k space is plotted for the four systems **19–22**. The Fermi level at 20 e/RhC_2 unit is marked with an arrow. In the case of **19** the double π and δ bands are drawn with double-dotted dashed lines. Thus, in **19**, **20**, and **22** we have displayed the five d bands as well as the two C_2 π^* bands. The similarity between **19** and **22** is clear. In the case of **21** because there are twice as many atoms in the unit cell, we have twice as many orbitals at any one k point. By unfolding,[19] we see though here too there is a great similarity to the bands in **19** and **22**. Finally, the two bands of local δ symmetry in **22** and the four such bands in **21** are indicated by double- and quadruple-dotted dashed lines.

orbitals thus replace the C_2 π^* frontier orbitals found in the isolated C_2 unit.

Let us now turn to the σ fragments shown in Figure 12c. In this figure we have chosen to assemble our orbitals differently,

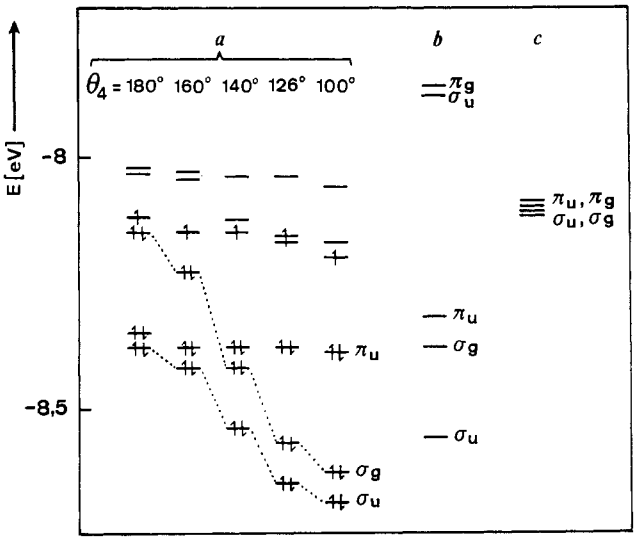

Figure 11. Study of the Rh_5C_{12} molecular orbitals near the Fermi level as a function of the angle θ_4. In (a) we show how the orbitals near the Fermi level change as a function of θ_4. The actual value of this angle (126°) is included. Filled molecular orbitals are indicated by arrows in the standard fashion. We trace with dotted lines the two orbitals that evolve the most as θ_4 changes. It may be seen that between θ_4 = 126 and 180° these two doubly occupied orbitals change their contribution to the total binding energy by a total of 1.6 eV. The comparison with Figure 7 shows that this represents somewhat more than the entire difference in the total energies. The symmetry labels π and σ refer to reflection through the plane of the Rh_5C_{12} unit. The sublabels are g (gerade) and u (ungerade) with respect to the inversion center at Rh1. Parts b and c show the frontier orbitals of the Rh_5C_8 fragment and the two C_2 fragments, respectively.

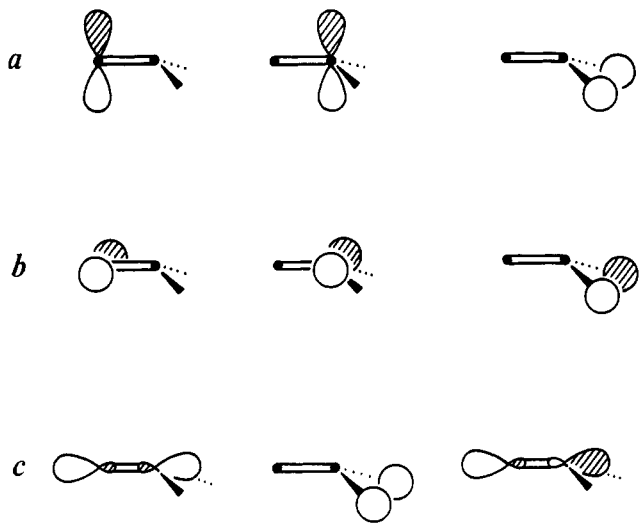

Figure 12. Orbitals used in accounting for the effect of the Er atoms on the C_2 frontier orbitals of **34**. Parts a and b show the C_2 π atomic orbitals and their Er s orbital counterparts. Part c shows the outward-pointing C_2 σ orbitals and their Er s counterpart.

in order to take into account the fact that the outward pointing s and p hybridizations on each carbon atom do not interact strongly with one another. Once again the three orbitals interact in a fashion analogous to that of the three π orbitals in the allyl unit. This time though the Er s orbitals are the central ones, and after interaction our central fragment orbital is of the form **39**, which

39

corresponds to a perturbed C_2 σ nonbonding orbital (**5**). It is the other frontier orbital of the C_2 fragment.

Table VI. Extended Hückel Parameters

atom	orbital	H_{ii}, eV	$\zeta(C_1)$	$\zeta(C_2)$
Er	6s	−6.0	2.00	
	6p	−4.0	2.00	
	5d	−7.0	3.50 (0.7734)	1.30 (0.4569)
Rh	5s	−8.0	2.14	
	5p	−4.5	2.10	
	4d	−11.0	4.29 (0.7765)	1.381 (0.4587)
C	2s	−21.4	1.63	
	2p	−11.4	1.63	

The effect of the Er atoms is now clear. The frontier orbitals of the C_2 units are less heavily weighted on the side where the Er atoms lie. Whenever a Rh atom lies on this side, the Rh–C bond is therefore weakened.

Finally it should be noted that this disproportionation of carbon orbital character is accomplished by a reduction in the orbital size on the one carbon atom and not by an increase in the orbital size of the other carbon atom. For example, the coefficients of the two atomic carbon orbital coefficients in the C_2 π^* orbital are ±0.837 when the C–C distance is set at 130 pm and the extended Hückel parameters given in Table VI are used. Under the influence of a pair of Er atoms like that shown in **34** these coefficients become 0.799 and −0.667 for respectively the carbon atoms far from and close to the Er atom.

In addition to the arrangement of Er atoms shown in **34**, there are two types of Er positions found in the $Er_8Rh_5C_{12}$ structure. These are **40** and **41**. It may be seen that effect of the lone Er

40 **41**

atom of **41** on the C_2 fragment orbitals will be similar to the effect of the pair of Er atoms in **34**. For example, in **41** the C_2 π^* carbon orbital coefficients shift to the values of 0.770 and −0.696 for respectively the carbon atoms far from and close to the Er atom. (We fixed the Er–C bond length to 240 pm.) These values are similar to the values reported for **34** in the previous paragraph. On the other hand, **40** presents one twist not present in the other arrangements. Perhaps the most important C_2 fragment orbital vis-à-vis Rh–C bond formation is the fragment orbital **5**. In **40**, unlike in **34** or **41**, this fragment orbital points away from the Er atoms. Hence, Er atoms such as those in **40** do not effect greatly the σ outward-pointing orbital **5**. Thus, for example the p-orbital coefficients of the carbon atom near the respective Er atoms shown in **34**, **41**, and **40** are respectively 0.548, 0.556, and 0.633 for this fragment orbital. This last value is not very different from the isolated C_2 fragment coefficient, which is 0.649. Thus, Er atoms like those in **40** have overall a weaker effect on Rh–C bonds.

We now turn to consider the $Er_8Rh_5C_{12}$ system as a whole. The Er atom positions are given in Figure 8. It may be seen that surrounding each C_2 pair are many Er atoms. Surrounding C1–C2 are for example the Er atoms 9/10, 15/16, and 11/12. What is the cumulative effect of all these Er atoms? To answer this question, it is useful to note the following result from second-order perturbation theory. The overall normalized correction to the orbital coefficient of the unperturbed orbital in second-order theory is just the linear sum of each of the perturbation corrections.[14] Hence, to calculate the effect of the three pairs of Er atoms on the p character of the outward-pointing σ orbital, we need for an approximate answer merely to add up each of the individual corrections. As an example, we consider the change in the orbital character of the outward-pointing σ orbital **5** brought about by the inclusion of multiple pairs of Er atoms. In particular we consider the arrangements **42** and **43**, which may be seen to be

42 **43**

(14) See for instance: Landau, L. D.; Lifshitz, E. M. *Quantum Mechanics*; Pergamon: Oxford, England, 1965; p 132.

Table VII. Changes in the C_2 Fragment Orbital **5** Induced by the Presence of Er Atoms

structure	s coeff	p coeff
	0.228	0.649
	0.174	0.635
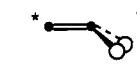	0.221	0.674
	0.142	0.548
	0.151	0.586
	0.133	0.592

[a] The atomic orbital coefficient of the carbon atom with an asterisk is given.

built up from **34** and **40**. In Table VII we list the s and p coefficients for the various combination forms. It may be seen that the linear sum rule is qualitatively correct.

In Figure 8 we gave the positions of the Er atoms relative to the Rh_5C_{12} chain. It may be seen that the Er atoms 7–10, 15, and 16 have positions of the type **34**, while the Er atoms 1–6, 11, and 13 lie in positions like that of **40**. Our calculations show that the effect of the Er atoms 19 and 20 on the bonds d_3, d_4, and d_5 is slight, and the effect of the Er atoms 9, 10, 15, and 16 on d_1 and d_2 is approximately cumulative. Thus, we find the Rh–C bonds d_1, d_2, and d_5 to be most affected by the inclusion of the Er atoms. Little change is expected for d_3 and d_4. An examination of Table V shows this to be true.

Conclusion

The band structure of several other ternary carbides will be reported elsewhere.[6] The systems studied include U_2NiC_3 and the $LnTC_2$ phases (Ln = lanthanoids, T = Fe, Co, Ni). In these systems we find that transition-metal–carbon bond distances and bond angles are correctly predicted by our extended Hückel treatment even when the positions of the lanthanoid and uranium atoms are ignored.

In the present work we have found that in the $Er_8Rh_5C_{12}$ system the Er atoms must be taken into account to understand both the Rh–C distances and the bond angles. Nevertheless, the effect of the Er orbitals is merely one of the fine-tuning. The interactions that bind the Rh and C atoms to one another remain 2-fold. First the C_2 bonding and nonbonding orbitals interact with the Rh s and p orbitals and second the C_2 π^* orbitals interact with the Rh d orbitals.

Therefore, our model is identical with the one used in accounting for the traditional molecular organometallic compounds.[15] Thus, in $SmRhC_2$, **8**, the C_2 fragments may be thought of as acetylenes in which the C–H bond has been replaced by a Rh–C bond. Each Rh atom therefore receives four electrons from the C_2 unit, which is side-bound, and two electrons from each of the end-bound C_2 pairs. The Rh atoms may be counted as Rh^-, and therefore we find 18 e around each transition metal. Similarly in the case of $Er_8Rh_5C_{12}$ we find that our central Rh receives two electrons from each of the C_2^{2-} units to which it is end-bound. Hence, were the Rh atoms in the −1 oxidations state, we would have a 14 e Rh that is approximately linearly coordinated. (This would correspond to the 20 e/RhC_2 unit in Figure 9).

Acknowledgment. We thank the Alexander von Humboldt Foundation for a stipend to S.L. The extended Hückel programs used in this work here originally developed by R. Hoffmann and

(15) A classic study of the C_2 dimer interaction (in the form of ethylene) with transition metals in molecular species is given in: (a) Hoffmann, R.; Albright, T. A.; Thorn, D. L. *Pure Appl. Chem.* **1978**, *50*, 3. A more recent example is: (b) Jorgensen, K. A.; Hoffmann, R. *J. Am. Chem. Soc.* **1986**, *108*, 1867.

his co-workers and brought into their present state by M.-H. Whangbo, T. Hughbanks, S. Wijeyesekera, M. Kertesz, C. N. Wilker, and C. Zheng. S.L. thanks Dr. G. Miller for providing us with copies of the programs and a reviewer, Dr. W. Tremel, and Prof. T. Hughbanks for their helpful comments and discussions. This work was supported by the Fonds der Chemischen Industrie.

Appendix

The extended Hückel method[16] was used in all calculations. The atomic parameters of our study are listed in Table VI. The Coulomb parameters of Er are of some interest. Values for rare-earth-metal d orbitals in previous extended Hückel studies[3c,17] range from −6.1 to −8.2 eV. The latter value would place the Er d orbitals at the same level as the C_2 π^* orbitals. In certain self-consistent studies it has been found the C_2 π^* level is filled while the rare-earth-metal levels are empty.[3d] Finally, when one compares the C_2 bond lengths of La_2C_3 and LaC_2 one finds that the C_2 bond length does not change more than 6 pm.[3e,18,19] In view of the above we place the rare-earth-metal d H_{ii} at −7 eV. We have verified that slightly lower values do not alter the overall picture presented in the current work.

Registry No. $Er_8Rh_5C_{12}$, 119147-24-9.

(16) Hoffmann, R. *J. Chem. Phys.* **1963**, *39*, 1397. (b) Whangbo, M. H.; Hoffmann, R. *J. Am. Chem. Soc.* **1978**, *100*, 6093. (c) Ammeter, J. H.; Bürgi, J.-B.; Thibeault, J. C.; Hoffmann, R. *J. Am. Chem. Soc.* **1978**, *100*, 3686.

(17) (a) Ortiz, J. V.; Hoffmann, R. *Inorg. Chem.* **1985**, *24*, 2095. A recent study on actinoide complexes is: (b) Tatsumi, K.; Nakamura, A.; Hofmann, P.; Hoffmann, R.; Moloy, K. G.; Marks, T. J. *J. Am. Chem. Soc.* **1986**, *108*, 4467.

(18) Simon, A. *J. Solid State Chem.* **1985**, *57*, 2.

(19) Atoji, M. *J. Chem. Phys.* **1961**, *35*, 1950. Atoji, M. *J. Chem. Phys.* **1961**, *35*, 1960.

(20) Burdett, J. K. *Prog. Solid State Chem.* **1985**, *15*, 173.

Contribution from the Anorganische Chemisch Laboratorium and Laboratorium voor Kristallografie, Universiteit van Amsterdam, J. H. van't Hoff Instituut, Nieuwe Achtergracht 166, 1018 WV Amsterdam, The Netherlands, and Afdeling Theoretische Chemie, Vrije Universiteit, De Boelelaan 1083, 1081 HV Amsterdam, The Netherlands

Structural, Spectroscopic, and Theoretical Studies of Novel d^6 *fac*-$Re(CO)_3LBr$ (L = Dithiooxamide) Complexes

Peter C. Servaas,[†] Derk J. Stufkens,*[,‡] Ad Oskam,[‡] Pieter Vernooijs,[§] Evert Jan Baerends,[§] Dirk J. A. De Ridder,[∥] and Caspar H. Stam[∥]

Received November 11, 1988

This article describes the syntheses and X-ray structures of three novel complexes $Re(CO)_3(DTO)Br$ (DTO = dithiooxamide), which differ in the dihedral angle θ between the thioamide groups of their DTO ligands. The structural data have been used for LCAO-Xα MO calculations on the model complex $Re(CO)_3(H_2\text{-DTO})Br$. Major differences in the structures and electronic absorption spectra are interpreted with the use of MO diagrams, orbital contour plots, calculated electronic interactions, and steric properties of the complexes. The X-ray and theoretical data show that no bonding interaction exists between the π orbitals of the thioamide groups at any dihedral angle. The thioamide π^* orbitals on the other hand interact at not too large dihedral angles, and this interaction causes the appearance of two intense electronic transitions. The predominantly Re(5d) → DTO(π^*) character of these transitions deduced from the theoretical data is confirmed by the resonance Raman spectra. The results of the MO calculations together with the X-ray structure determination of $Re(CO)_3(Cycl\text{-DTO})Br$ show that π-back-bonding from the $Re(CO)_3Br$ moiety to the lowest π^* orbital of the DTO ligand mainly occurs via an orbital with substantial (69%) Br 4p character.

Introduction

Most studies of transition-metal complexes having a lowest metal to ligand charge-transfer (MLCT) state have dealt with compounds containing members of the α-diimine family such as 2,2′-bipyridine and 1,10-phenanthroline. Our contribution in this field consisted of several studies on a series of mononuclear and dinuclear transition-metal carbonyl complexes containing these ligands.[1-6] Special attention was paid to the characterization of the metal to α-diimine charge-transfer transitions by means of resonance Raman spectra in relation to the photochemistry of these complexes.[7-10]

In all complexes studied the low-energy MLCT transitions were directed to the lowest π^* orbital of the α-diimine. Figure 1A shows the structure of *N*,*N*′-R_2-1,4-diaza-1,3-butadiene (R-DAB), which is the most simple representative of these α-diimines.

Another class of ligands also possessing a low-lying π^* orbital are the N,N′-R_2-substituted dithiooxamides (abbreviated as R_2-DTO), the general structure of which is shown in Figure 1B.

Structure determinations of several of these R_2-DTO ligands (R = Et, iPr, H)[11-14] have confirmed the planar geometry of these ligands. From the C–N and C–S bond lengths in these structures it was concluded that the R_2-DTO ligands consisted of two coupled thioamide functions. However, the relatively long central C–C

* To whom correspondence should be addressed.
† Present address: Fasson Nederland, Specialty Division, P.O. Box 28, 2300 AA Leiden, The Netherlands.
‡ Anorganisch Chemisch Laboratorium, Universiteit van Amsterdam.
§ Afdeling Theoretische Chemie, Vrije Universiteit.
∥ Laboratorium voor Kristallografie, Universiteit van Amsterdam.

(1) Balk, R. W.; Stufkens, D. J.; Oskam, A. *Inorg. Chim. Acta* **1978**, *28*, 133.
(2) Kokkes, M. W.; Stufkens, D. J.; Oskam, A. *J. Chem. Soc., Dalton Trans.* **1983**, 439.
(3) Servaas, P. C.; van Dijk, H. K.; Snoeck, Th. L.; Stufkens, D. J.; Oskam, A. *Inorg. Chem.* **1985**, *24*, 4494.
(4) Andrêa, R. R.; Luyten, H.; Vuurman, M. A.; Stufkens, D. J.; Oskam, A. *Appl. Spectrosc.* **1986**, *40*, 1184.
(5) Stufkens, D. J. Steric and Electronic Effects on the Photochemical Reactions of Metal-Metal bonded Carbonyls. In *Stereochemistry of Organometallic and Inorganic Compounds*; Bernal, I., Ed.; Elsevier: Amsterdam, 1989; Vol. 3.
(6) van Dijk, H. K.; Stufkens, D. J.; Oskam, A. *J. Am. Chem. Soc.* **1989**, *111*, 541.
(7) Balk, R. W.; Snoeck, Th. L.; Stufkens, D. J.; Oskam, A. *Inorg. Chem.* **1980**, *19*, 3015.
(8) Balk, R. W.; Stufkens, D. J.; Oskam, A. *J. Chem. Soc., Dalton Trans.* **1981**, 1124.
(9) van Dijk, H. K.; Servaas, P. C.; Stufkens, D. J.; Oskam, A. *Inorg. Chim. Acta* **1985**, *104*, 179.
(10) Servaas, P. C.; Stufkens, D. J.; Oskam, A. *Inorg. Chem.* **1989**, *28*, 1780.
(11) Drew, M. G. B.; Kisenyi, J. M.; Willey, G. R. *J. Chem. Soc., Dalton Trans.* **1982**, 1729.
(12) Drew, M. G. B.; Kisenyi, J. M.; Willey, G. R.; Wandiga, S. O. *J. Chem. Soc., Dalton Trans.* **1984**, 1717.
(13) Wheatley, P. J. *J. Chem. Soc.* **1965**, 396.
(14) Mo, F.; Thorkildsen, G. *Acta Crystallogr., Sect. A* **1984**, *A40*, C160.

0020-1669/89/1328-4104$01.50/0